Finger vein recognition based on deformation information

Xianjing MENG[1], Xiaoming XI[1], Gongping YANG[2] & Yilong YIN[2*]

[1]*School of Computer Science and Technology, Shandong University of Finance and Economics, Jinan* 250014, *China;*
[2]*School of Computer Science and Technology, Shandong University, Jinan* 250101, *China*

Abstract The measurement of the vessel pattern in fingers is a superior method for identifying individuals owing to its convenience and the security it offers. We introduce in this paper a new perspective to accomplish finger vein recognition. This method, which regards deformations as discriminative information, is distinct from existing methods that attempt to prevent the influence of deformations. The proposed technique is based on the observation that regular deformation, which corresponds to a posture change, can only exist in genuine vein patterns. In terms of methodology, we incorporate optimized matching to generate pixel-based 2D displacements that correspond to deformations. The texture of uniformity extracted from the displacement fields is taken as the final matching score. Evaluated on two publicly available databases, PolyU and SDU-MLA, extensive experiments demonstrated that the discriminability of the new feature derived from deformations is preferable. The equal error rate (EER) achieved is the lowest compared to that of state-of-the-art techniques.

Keywords finger vein recognition, deformations, optimized matching, displacement, texture of uniformity

1 Introduction

In the information age, it is very important to be able to accurately determine the identity of a person. Therefore, biometric authentication has received increasing attention from researchers. Biometric authentication or biometrics [1, 2] refers to an automatic method for recognizing a person using behavioral or physiological features. As intrinsic human features, biometric patterns are more reliable than traditional authentication techniques based on contents (code, password, etc.) or possessed objects (certificate, key, smart card, etc.) and offer more acceptable user experiences [3]. At present, personal verification based on biometrics is widely adopted for door access control, security systems, forensics, and so forth.

Finger veins are subcutaneous structures that are randomly spread along a finger. The vein patterns are believed to be distinctive even between identical twins and remain constant throughout the adult years [3, 4]. Biometric authentication based on finger veins demonstrates many advantages compared to other biometrics. The most cited merits for finger vein recognition are three-fold [3, 5, 6]: First, the images are captured in a non-contact way, which ensures sanitary conditions and user-friendliness. Second, the recognition is based on structures hidden in a live body; thus, it is very difficult to steal

---

* Corresponding author (email: ylyin@sdu.edu.cn)

finger vein patterns and offers anti-spoofing capabilities. Third, there are multiple fingers that can be authenticated; hence, the fusion of more than one finger can improve both security and performance. At present, identification based on finger veins has received considerable attention from researchers and has been successfully applied in commercial uses [7,8].

Typically, a finger vein recognition system consists of four main procedures: image capturing, preprocessing, feature extraction, and matching. In particular, image capturing visualizes the veins in a finger. Preprocessing mainly involves image enhancement and region-of-interest (ROI) segmentation. Feature extraction entails analyzing the characteristics of the finger vein for representation, and matching measures the similarity of two finger vein images.

In the last two decades, finger vein recognition has been extensively explored. A considerable amount of work has been reported in the literature, which can be roughly divided into four categories according to the feature extraction procedure: local pattern-based methods, network-based methods, minutiae-based methods, and machine-learning-based methods. (1) Local pattern-based methods extract pixel-based features for the whole ROI, then match the features using a pixel-to-pixel technique. These kinds of methods include local binary pattern (LBP) [9] and its variants, such as local derivative pattern (LDP) [9] and local directional code (LDC) [10]. These methods extract features from not only vessel regions, but also non-vessel regions, so the performance may be inferior when vessels are sparse. On the other hand, their pixel-to-pixel matching technique is extremely sensitive to deformations. (2) Network-based methods extract features from segmented blood vessels and then match them according to the similarity of vein patterns. Typical methods are mean curvature (MeanC) [11], repeated line tracking (RLT) [12], even Gabor with morphological operation (EGM) [13] and so forth. Accurate vessel segmentation is difficult; therefore, the performance of network-based finger vein recognition remains unsatisfactory. (3) The minutiae-based methods, e.g., modified Hausdorff distance (MHD) with minutiae feature matching [14] and singular value decomposition (SVD)-based minutiae matching (SVDMM) [15], define the cross and end points of vessels as minutiae and then calculate their similarity according to the local features around them. However, the limited and spurious minutiae in a finger vein image hinder performance. (4) Methods based on machine learning mainly include principal component analysis (PCA) [16] and its variants, namely two-directional and two-dimensional PCA ($(2D^2)$PCA) [17,18], and linear discriminant analysis (LDA) [19]. As recognition is a multi-class classification problem, training images are not always available to train the transformation matrix in these methods, which means that the performance of these methods is not satisfactory.

Although the performance of finger vein recognition has been promoted by the above-mentioned approaches, dramatic performance improvement has not been achieved. Finger vein recognition continues to remain a challenging task due to image quality issues and deformations [9,20]. As for image quality, because finger veins are part of the blood circulation system within the subcutaneous tissue, they cannot be observed using visible light. Thus, near infrared (NIR) light (700–1000 nm) is often used in finger vein image acquisition, because the NIR rays can penetrate human tissues and are absorbed by the hemoglobin in the veins. However, images of a finger captured under NIR light contain not only the vein patterns, but also irregular shading produced by various thicknesses of finger bones and muscles [21–23], which can result in the detection of ambiguous or incomplete vessel structures. With respect to the deformations, since the finger is a kind of non-rigid object and is arranged in a non-contact way during image capturing [24], the finger vein images are adversely affected by various deformations, as shown in Figure 1. The deformations can be categorized as follows: (1) in-plane translations and rotations, (2) out-of-plane rotations, (3) global or local expansion or contraction due to muscle tension and joint states. Furthermore, the bloodstream can vary as a function of different human physical states. Mostly, the presence of different kinds of deformation complicates an image, and can seriously degrade the performance of the recognition system.

In combination, the occurrence of both image quality problems and deformations has a negative influence on the recognition system. The image quality problem is usually solved by image restoration [22] or blood vessel enhancement [25] in the preprocessing operation, whereas the deformation problem has been considered at each stage of the process by researchers. We notice that in all cases, researchers
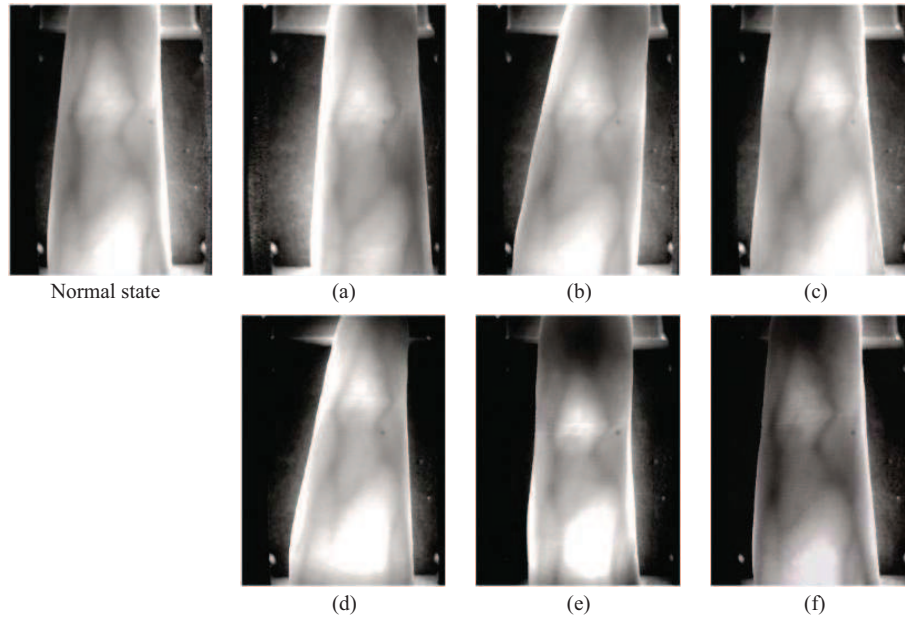
Figure 1 Various kinds of deformations of the same finger. (a) and (b) Finger vein images affected by in-plane translation and rotation; (c) and (d) examples of out-of-plane rotation; (e) bent finger; (f) captured after exercise, and exhibits low intensity.

try to reduce or eliminate the influence of deformations by careful ROI segmentation [21, 25–27], robust feature extraction [10–13, 15, 28–32], or statistical analysis [33]. All of these techniques can improve the performance of finger vein recognition, but in most cases can only partially solve the problem. Existing ROI extraction methods usually have similar objectives despite the various detailed operations, which is to adjust the skew and locate the phalangeal joints in order to further determine the benchmark region. Obviously, these techniques can overcome some of the rigid deformations, such as in-plane translations and rotations, whereas they have a negligible effect on other deformations. Extracting features from segmented vessel networks [11–13, 15, 28] is an intrinsic solution to decrease the influence of deformations because the topology of vessels never changes. However, segmenting a well-networked finger vein pattern from an image is usually impractical when the image contrast is low, therefore the performance is still unsatisfactory [25]. Attempts to prevent the segmentation of vessel networks have led to the introduction of local pattern-based methods [10, 29, 31, 32] for finger vein recognition; however, these have not been successful in the case when various deformations exist due to the use of a pixel-to-pixel matching scheme.

In this paper, we introduce a new perspective to overcome deformations, which is to regard the deformations as discriminative information rather than as a negative influence. Pixel-based features are adopted; thus, simultaneous blood vessel extraction, which is sensitive to image quality, is prevented from occurring. Our approach is based on the observation that the pixel-based displacements generated in the matching process, which correspond to the various deformations, can convey discriminative information. The information that enables distinction between genuine and imposter matching is as follows: (1) the displacements for a pixel and its neighbors are similar in genuine matching because pixels in a local region tend to be similar in deformation; (2) the number of pixels that have the same displacement tends to be larger in genuine matching because two genuine images share the same finger vein structures. Note that, the pixel-based displacements can reflect various kinds of deformations categorized above.

We obtain the pixel-based displacements by treating the matching process as a pixel-based optimization process [34]. Thus, the dense correspondences between two images are obtained in a flexible way. Then, we regard the displacement matrices generated from genuine and imposter matching as different patterns, and extract texture features to determine whether they are from the same finger. Accordingly, the proposed method consists of three stages: In the first stage, the dense scale invariant feature transform (SIFT) descriptor [35] is adopted as the pixel-based feature for its powerful discriminability. In the second

stage, the matching process is simulated as an optimization objective; consequently, the displacements for each pixel are generated. Finally, the texture feature of uniformity [36] is extracted as the final matching scores from the displacement matrix.

The contributions of the proposed method are as follows:

(1) A new perspective to accomplish finger vein recognition. Contrary to traditional measures, we treat the deformations as useful information that contribute to recognition rather than as a negative influence. Thus, the deformation problem is solved. The various appearances of images from one finger can result in unstable similarities, but they still correspond. This ensures robustness of recognition based on deformations.

(2) Pixel-based optimization to access deformations. We consider the matching process as a pixel-based optimization procedure based on dense local features. Thus, the extraction of blood vessels is prevented. The proposed method is much more discriminative than vessel-network-based methods because the displacement fields generated encode not only the vessel network regions.

(3) Adoption of the uniformity feature extracted from the displacement fields to indicate whether they are genuine.

The remainder of this paper is organized as follows. The main theory of this paper, i.e., the relationship between deformations and 2D displacements and the characteristics of 2D displacements, are fully analyzed in Section 2. In Section 3, the recognition based on deformations, from pixel-based optimized matching to the extraction of the texture of uniformity, are introduced. We then report extensive experimental results in Section 4. Finally, the paper is concluded in Section 5.

2 Main idea

This section presents the analysis of the characteristics of deformations and the possibility of extracting features from displacements. As mentioned above, the finger is a three-dimensional object and any posture changes during image capturing can cause deformations in a two-dimensional finger vein image. That is, one finger vein image corresponds to one posture of the finger; similarly, one posture change corresponds to differences, i.e., deformations, of two images.

The matching procedure of a finger vein recognition system takes as its input two images A and B to assess their similarity. As for the pixel α from the same position of a finger, the relationship of A_α and B_α is as follows:

$$A_\alpha(x, y) = B_\alpha(x + \Delta x, y + \Delta y) + \varphi, \tag{1}$$

where (x, y) denotes the position of pixel α in image A, $(x + \Delta x, y + \Delta y)$ denotes the position of pixel α in image B, and Δx and Δy represent displacements in the horizontal and vertical directions, respectively. φ demonstrates the difference between the pixel-based features of two pixels. At the image level, the relationship of image A and B can be represented as

$$A = D_{\text{func}}(B, \Psi) + \Phi. \tag{2}$$

Here, D_{func} indicates the transformation between image A and B. If A and B are genuine, D_{func} represents the posture change between them. If they are imposter images, the transformation will be complex. Further, $\Psi = (\Delta X, \Delta Y)$ represents the displacement matrix in the horizontal and vertical directions and Φ denotes the difference matrix of pixel-based features.

Most existing finger vein recognition methods are based on the intuitive observation that if the difference Φ between pixel-based features tends to be small, images A and B tend to be similar. In this case they would not allow detection of the difference of transformations between genuine and impostor matching. In this study, we try to explain the difference and use it to facilitate recognition. We noticed that the displacements Ψ generated during genuine matching represent the deformations of the finger, which correspond to a posture change in genuine matching, but can be irregularly spread in imposter matching. The pixel-based displacement has two parameters: displacement distance s and orientation θ. We provide an example to elaborate the main idea, as shown in Figure 2. In Figure 2, two sets of
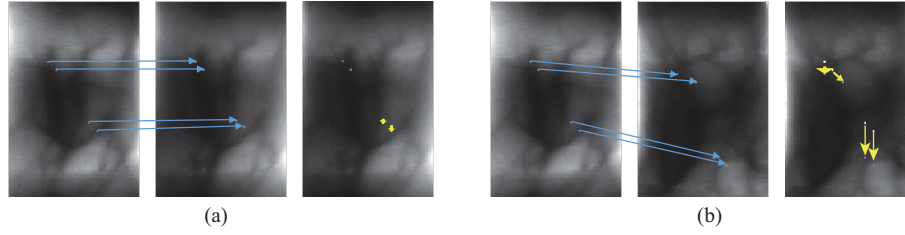
Figure 2 (Color online) Displacements generated in genuine and imposter matching show discriminative information. Yellow arrows indicate the pixel-based displacements. (a) Genuine matching: the four matched pixels have similar displacements, i.e., the displacements of the four positions are small and similar in direction; (b) imposter matching: the displacements of the four matched pixels vary, i.e., the displacements are large in distance and in various directions.

images of the same finger vein are compared: one set is from the same finger (genuine matching); the other is from a different image (imposter matching). The genuine matching set, (Figure 2(a)), indicates that the pixels and their neighbors have similar displacements, whereas the displacements are irregular in imposter matching.

For simplicity, we decouple the displacement into horizontal and vertical directions denoted as $(\Delta x, \Delta y)$, then s and θ can be represented as

$$s = \sqrt{\Delta x^2 + \Delta y^2}. \tag{3}$$

$$\theta = \begin{cases} \arccos \dfrac{\Delta x}{s}, & \Delta y \geqslant 0, \\ \pi - \arccos \dfrac{\Delta x}{s}, & \Delta y < 0. \end{cases} \tag{4}$$

In this paper, we use $(\Delta x, \Delta y)$ to represent the pixel-based displacement. Thus, we have two displacement matrices in the horizontal and vertical directions ΔX and ΔY, respectively. The displacement matrix generated from genuine and imposter matching has different characteristics, i.e., in a genuine matching, the displacement matrix is uniformly distributed with regions of similar displacement gathered together, whereas in an imposter matching, the displacements are irregularly spread: (1) All values of displacements in genuine matching remain in a small interval, whereas displacement values in imposter matching vary across a much larger interval because irrelevant pattern matching introduces additional uncertainties. (2) Regions of the same displacement values in genuine matching tend to be larger in terms of area covered than in imposter matching.

The displacements can also be robust on consideration that, even though two genuine images are sometimes not similar in appearance, the displacements are still uniformly spread. The above analysis enables us to determine the possibility and potentiality of using the deformations to perform finger vein recognition.

3 Methodology

The proposed method comprises several steps, as shown in Figure 3. First, the finger vein images are preprocessed by ROI segmentation and image enhancement, which correspond with our previous work. As mentioned in the introduction, the ROI segmentation can adjust some of the global deformations, such as in-plane translations and rotations, as illustrated in Figure 4. Then, pixel-based dense SIFT descriptors are extracted to represent each image. Next, optimized matching is employed to generate the pixel-based displacement. Finally, the texture of uniformity is calculated as the final matching score.

3.1 Dense SIFT descriptor

The original SIFT descriptor, which consists of both feature extraction and saliency detection components, is a kind of sparse descriptor in characterizing local gradient information. In this paper, we use the dense
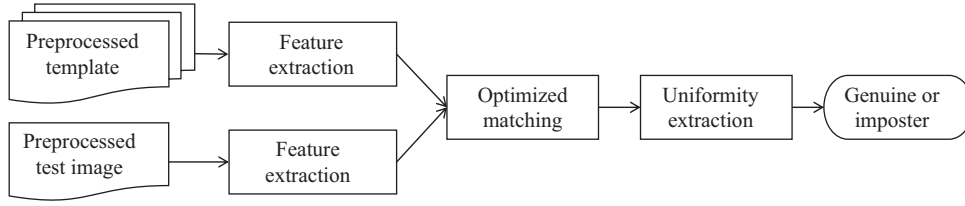
Figure 3 Flowchart of the proposed method.

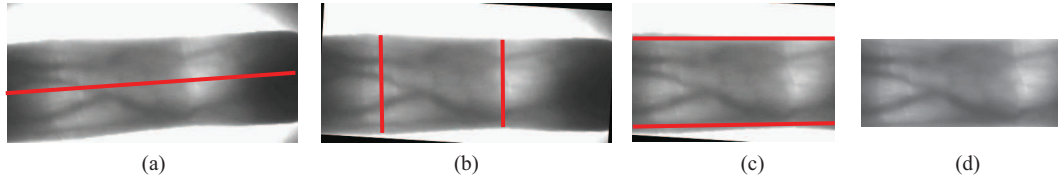(a)   (b)   (c)   (d)

Figure 4 (Color online) Illustration of the ROI extraction. (a) Center line detection of the finger vein image, according to which the skew can be adjusted; (b) finger joints detection; (c) internal tangents of the edges of the finger; (d) the ROI of the sample finger.

SIFT descriptor [35] to represent each pixel. The reason why this descriptor is adopted is that the dense SIFT is calculated in a large neighborhood; therefore, it represents a pixel more appropriately.

The extraction procedure is as follows: (1) for every pixel in an image, divide its 16×16 neighborhood into a 4×4 cell array; (2) quantify the orientation in each cell into 8 bins. Thus, for each pixel, a 128-dimensional (16 bins $\times$ 16 cell) vector is extracted.

3.2 Matching objective

In order to obtain the displacement matrices, the best match for each pixel needs to be found first. Then, the displacement for each pixel is generated simultaneously. The best match for a pixel must have the most similar features; however, if the best matches are irregularly spread, the two matched images still tend to be imposter images. Based on the above consideration, we take the matching process as an optimization problem [34]. Let s_1 and s_2 be the two dense SIFT images that need to be matched, with ε containing all the neighborhoods. The energy function, which consists of three parts, is defined as follows:

$$E(w) = \sum_p \|s_1(p) - s_2(p + w(p))\|_1 \tag{5}$$

$$+ \frac{1}{\sigma^2} \sum_p \left(\Delta x^2(p) + \Delta y^2(p) \right) \tag{6}$$

$$+ \sum_{(p,q) \in \varepsilon} \min \left(\alpha |\Delta x(p) - \Delta x(q)|, d \right) + \min \left(\alpha |\Delta y(p) - \Delta y(q)|, d \right), \tag{7}$$

where $p = (x, y)$ represents the coordinate position of the current pixel, $w(p) = (\Delta x(p), \Delta y(p))$ denotes the 2D displacement for finding the optimal correspondence for a pixel, and $s_i(p)$ indicates the SIFT descriptor extracted at location p of image i. $\Delta x(p)$ and $\Delta y(p)$ are only allowed to be integers and are assumed to have L possible states, where L is the size of the search window. In addition, ε is the spatial neighborhood of a pixel (here a four-neighborhood structure is used).

The three parts of the function are, respectively, a data term that is used to calculate the similarity of two images after displacement, a displacement vector that should be as small as possible because it is necessary to select the best match from the surrounding vicinity, and a smoothness term that indicates that the adjacent pixels tend to have similar displacements. In the smoothness term, the thresholded L1 regularizer is used to preserve discontinuities in the images. A dual-layer loopy belief propagation is used as the base algorithm to optimize the objective function, and the parameter settings are fixed as $\sigma = 300$, $\alpha = 0.5$, and $d = 2$, which are the same as those in a previous report [34]. We retained the value $d = 2$
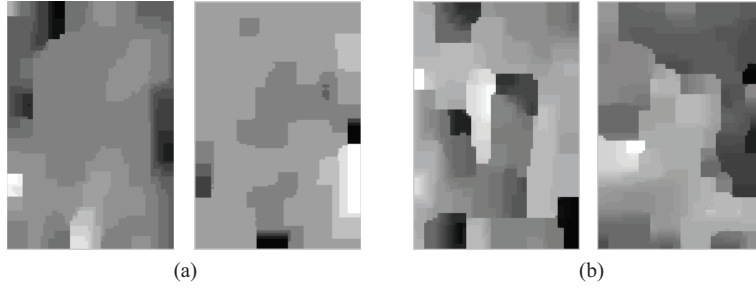
(a)   (b)

Figure 5   Displacement matrices of (a) genuine and (b) imposter matching.

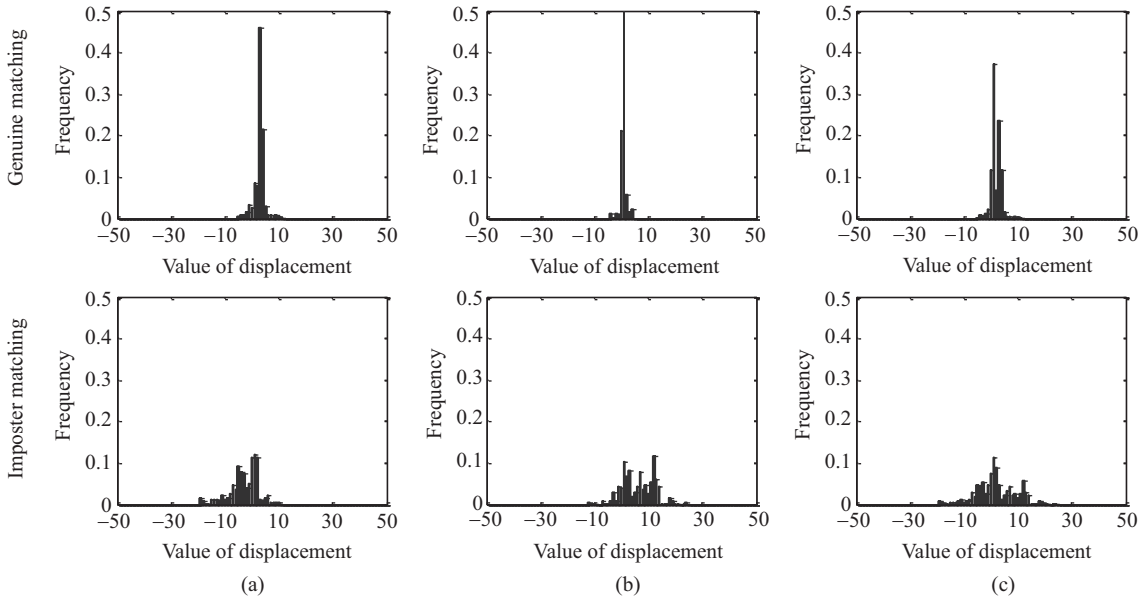(a)   (b)   (c)

Figure 6   Description of uniformity feature. (a) The normalized histogram of the horizontal direction; (b) the normalized histogram of the vertical direction; (c) the merged histogram of both directions.

because $d/\alpha = 4$ is usually used as the neighborhood number [15,34] or step size of the sliding window [9] in matching.

3.3   Displacement uniformity

The displacement matrices are derived from the optimized matching (as shown in Figure 5). In order to be displayed as an image, the displacements are normalized to the range of 0 to 255. We extract the texture feature of uniformity [36] from the displacement matrices to differentiate genuine matching from imposter matching. Let h_x and h_y be the histograms of the displacement matrices, as shown in Figure 6, where $h(i)$ denotes the number of pixels with displacement value i. Then the definition of uniformity is

$$f = \sum_{i \in l} \left(\frac{h_x(i) + h_y(i)}{2MN} \right)^2. \tag{8}$$

Here, M and N represent the height and width of the finger vein image, respectively. The value of l varies from $[\min(\Delta X, \Delta Y)$ to $\max(\Delta X, \Delta Y)]$. Correspondingly, the value of f is between 0 and 1. When the two matched images are from the same finger, the texture of the generated displacement field tends to be uniform, the uniformity is relatively large (in Figure 6, and the uniformity of genuine matching is 0.2278). Conversely, the texture of displacement fields from imposter matching is full of uncertainties. The uniformity tends to be small (in Figure 6, and the uniformity of imposter matching is 0.0511). The metric of uniformity can achieve the largest value, which is 1, when all the displacements are equal in value, and tends to be 0 when the range of displacement value tends to infinity.

Table 1 Verification performance by different methods on PolyU and SDU-MLA database

Method	PolyU database			SDU-MLA database		
	EER	FRR at-zero-FAR	FAR at-zero-FRR	EER	FRR at-zero-FAR	FAR at-zero-FRR
MO function	0.0310	0.2511	0.9183	0.0684	0.8936	0.9982
Proposed method	0.0053	0.2182	0.6674	0.0268	0.7152	0.9989

4 Experiments

4.1 Experimental material

The proposed method is evaluated on two publicly available finger vein databases: The first is from Hong Kong Polytechnic University (polyU) and the other is from the Machine Learning and Data Mining Lab at Shandong University (SDU-MLA).

The polyU database [13] includes high intra-class variances since unconstrained imaging was attempted during image collection. These images were captured from 156 volunteers over a time period of eleven months and included two separated sessions. Each volunteer contributed 12 images from the index and middle finger of the left hand, with 6 images of each finger. As only 105 volunteers presented themselves for the second session, only those finger vein images captured in the first session are considered in our experiment. Thus, the data set used in our experiment includes 1872 images.

The SDU-MLA finger vein database is a subset of the homologous multi-modal traits (SDUMLA-HMT) database [37]. This data set was captured from 106 subjects, of whom each contributed 36 images from the index, middle, and ring finger of both hands, with 6 images of each finger. Thus, the second data set used in our experiment consists of 3816 images. This database is captured in an uncontrolled way, and is more difficult to conquer.

Since the two databases were captured using different devices, the images have different characteristics. Accordingly, we preprocess the databases using different algorithms: the polyU database is preprocessed by using the sliding window method [27], and the SDU-MLA database is preprocessed by using the techniques described in [10]. The size of all the images is 96×64, with intensities normalized to the range from 0 to 255.

4.2 Compared with matching objective in verification mode

In this part, we present our evaluation of the performance of the proposed method in the verification mode. In [34], the authors utilized the output of the objective function to accomplish face recognition. Thus, we also compared our method with the output of the matching objective (MO) function. Note that, the output of the MO function can be very large, owing to the SIFT descriptor differences in the data term. We normalized the output of the MO function to $[0, 1]$ to facilitate visualization.

In this mode, we first acquired a set of matching scores by utilizing full matching in inter-class and intra-class matching. Consequently, there are 4680 ($312 \times C_6^2$) intra-class and 3493152 ($312 \times 6 \times 311 \times 6$) inter-class matching points in the PolyU database, respectively. In addition, there are 9540 ($636 \times C_6^2$) intra-class and 14538960 ($636 \times 6 \times 635 \times 6$) inter-class matching points on the SDU-MLA database, respectively. The distributions of genuine and imposter matching scores for the two databases of the proposed method and MO function are provided in Figures 7 and 8, respectively. Then, the performance of the proposed method is examined by computing the EER (equal error rate), FRR (false rejection rate) at-zero-FAR (false acceptance rate), and FAR at-zero-FRR, as in Table 1, with the receiver operational characteristic (ROC) curve for the two databases shown in Figure 9, respectively.

The distribution of the genuine and imposter matching scores on the PolyU database shown in Figure 7 indicate that the genuine and imposter matching scores of the proposed method are overlapped between 0.05 and 0.32, whereas for the MO function they are between 0.28 and 0.65, which is a much larger interval. Moreover, the imposter matching scores of the proposed method are mainly between 0 and 0.18, whereas the imposter matching scores of the MO function are generally between 0 and 0.66, which
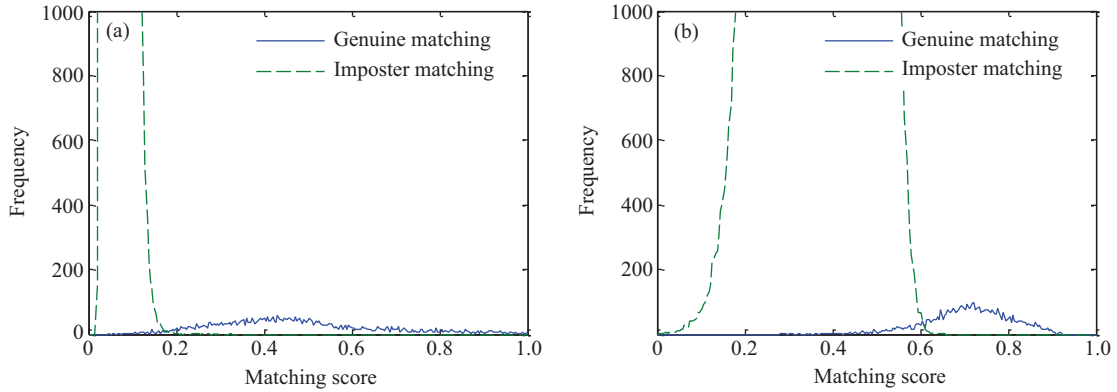
Figure 7 (Color online) Distribution of matching scores on the PolyU database. Score distribution of (a) proposed method and (b) MO function.
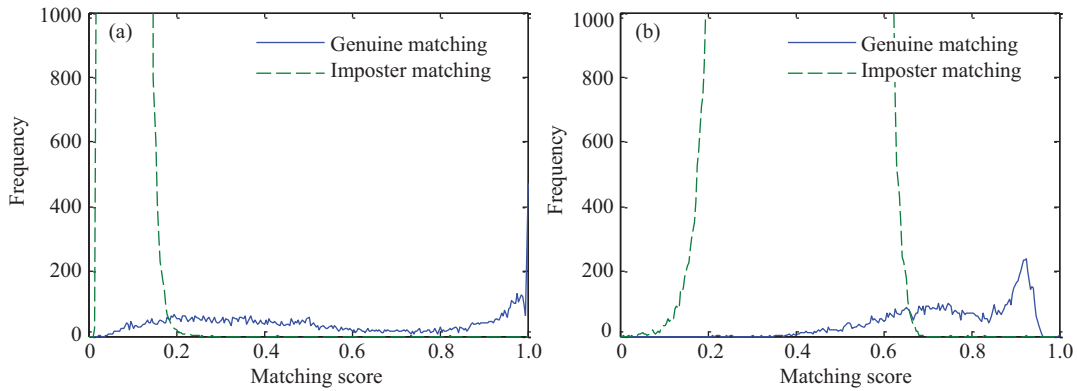

Figure 8 (Color online) Distribution of matching scores on the SDU-MLA database. Score distribution of (a) proposed method and (b) MO function.
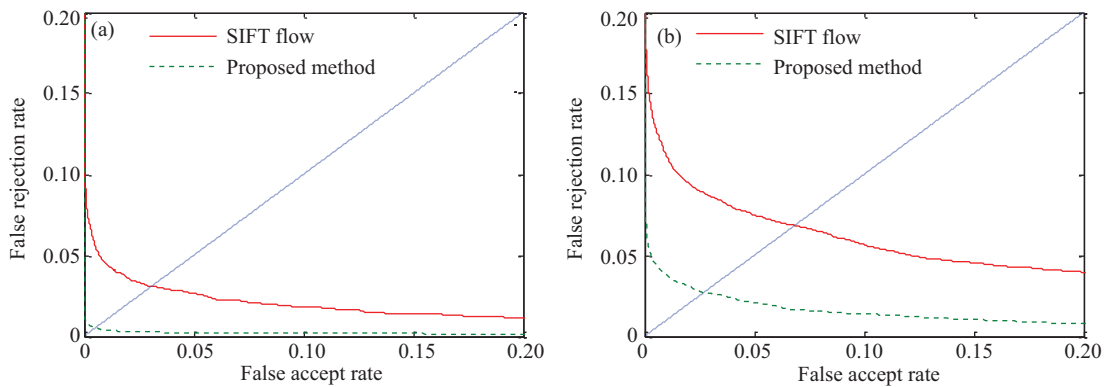

Figure 9 (Color online) ROC curves for the two databases: (a) PolyU database and (b) SDU-MLA database.

indicates that the proposed method enlarges the overall distances between the imposter and genuine matching scores and is relatively robust and tolerant toward a new and hard data set.

The SDU-MLA database consists of images that have various deformations and is much larger in scale. The distribution of genuine and imposter matching scores shown in Figure 8 shows that the overlapped score interval of the proposed method is between 0.02 and 0.3, which is much smaller than the range 0.2 to 0.7 of the MO function. Although the genuine scores of the proposed method vary due to intraclass variances, the imposter scores are mostly smaller than 0.2, which ensures high performance of the proposed method.

The ROC curve shown in Figure 9 and the performance in Table 1 show that the EERs of the proposed

Table 2 Time efficiency analysis of the proposed method

Method	Preprocessing (ms)	Feature extraction (ms)	Optimized matching (ms)	Feature extraction (ms)	Total (ms)
MO function	37.2	9.4	287.4	−	334
Proposed method	37.2	9.4	287.4	0.6	334.6

method and MO function are 0.0053 and 0.0310 on the PolyU database, respectively, and on the SDU-MLA database the corresponding values are 0.0268 and 0.0684, respectively. The EERs of the proposed method on both databases are much lower than the MO function, which indicates that the proposed method can more effectively represent the characteristics of each finger vein pattern and is robust in performance. The results in Table 1 indicate that the FRR at-zero-FAR and FAR at-zero-FRR of the proposed method on the PolyU database are both much lower than the MO function. On the SDU-MLA database, the FRR at-zero-FAR is also much lower with the FAR at-zero-FRR in proximity of 1 for both methods.

The experimental results demonstrate the discriminability of the deformations: First, Figures 7 and 8 show that the imposter matching scores are mainly between 0 and 0.2, which indicates that two imposter images cannot form a uniform posture change. This is consistent with the analysis in Section 2. Second, the genuine matching scores on the PolyU database in Figure 7 are more uniformly spread, whereas the genuine matching scores on the SDU-MLA database are irregularly spread from 0 to 1. This is consistent with the observation that there are many hard cases from the SDU-MLA, which on the other hand indicates the discriminability of the proposed feature.

In this part, we also present the analysis of the time efficiency of the proposed method, as shown in Table 2. The experiments are implemented using MATLAB, and conducted on a PC with a 3.6 GHz CPU and 4 GB main memory. Compared to recognition based on the MO function, the texture of uniformity extraction is added and the average time consumption is 0.6 ms. However, the MO function needs an optimization procedure, because the average matching time is 287.4 ms, which is relatively time consuming. Consequently, the overall time consumption of the proposed method is 334.6 ms. Since all the experiments were implemented on MATLAB, which is an integrated platform, the performance might still be improved. Moreover, if parallel computing was to be employed for the verification, real-time recognition could be achieved.

4.3 Compared with matching objective in recognition mode

In this experiment, we evaluated the proposed method in the recognition mode and compared it with the MO function. In the recognition mode, the class to which the input finger vein image belongs is unknown and has to be verified. In the experiment, we used the first three finger vein images of each class as the test images and randomly selected one finger vein image from the remaining three images of each class as samples. Consequently, there are 312 templates and 936 (312×3) probes on the PolyU database, and 630 templates and 1890 (630×3) probes on the SDU-MLA database. The probes are matched with all the templates. The rank of each probe is acquired by calculating the ranking of its true class matching score. This enabled us to obtain the cumulative match curves as shown in Figure 10. We repeated the experiment ten times in order to obtain an unbiased result. The average rank-one recognition rate and the maximum lowest rank for perfect recognition (the lowest rank when the recognition rate reaches 100%) are listed in Table 3. From the results, we can see that the proposed method achieves a recognition rate above 99% and varies in a very small interval on the PolyU database. In contrast, the rank-one recognition rate of the MO function is 93.82%, which is much lower and varies over a larger interval. Moreover, the lowest perfect rank of the proposed method, which is 25, is also much smaller than the 230 of the MO function. The result on the SDU-MLA database shows the same trends when the two methods are compared. The rank-one recognition rate of the proposed method is about 10% higher with the lowest rank about 150 smaller than for the MO function. The performance indicates that the proposed method is a superior candidate for the finger vein recognition task.
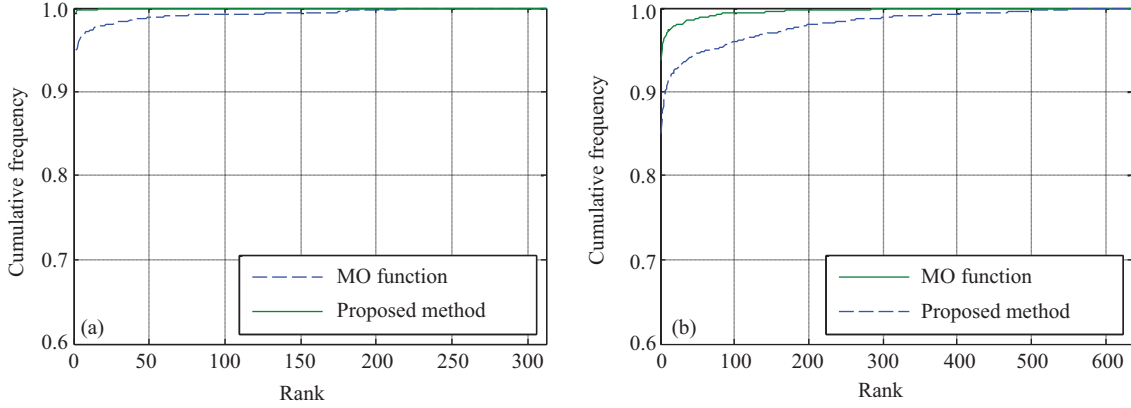
Figure 10 (Color online) Cumulative match curves by different methods: (a) PolyU database and (b) SDU-MLA database.

Table 3 Identification performance by different methods on PolyU and SDU-MLA database

Method	PolyU database		SDU-MLA database	
	Rank-one recognition rate	Lowest rank of perfect recognition	Rank-one recognition rate	Lowest rank of perfect recognition
MO Function	0.9382 ($\pm$0.0222)	230	0.8483 ($\pm$0.0158)	633
Proposed method	0.9940 ($\pm$0.0041)	25	0.9400 ($\pm$0.0074)	477

Table 4 Performance comparison with and without smooth term

Method	Verification mode			Recognition mode	
	EER	FRR at-zero-FAR	FAR at-zero-FRR	Rank-one recognition rate	Lowest rank of perfect recognition
Without smooth	0.0145	0.0754	0.9499	0.9810 ($\pm$0.0034)	224
Proposed method	0.0053	0.2182	0.6674	0.9940 ($\pm$0.0041)	25

4.4 Smooth term analysis

This part contains an analysis of the effectiveness of the objective function. First, we evaluate the effect of the smooth term by measuring the performance without it, using the same experimental setting as in Subsection 4.2 on the PolyU database. The EER and rank-one recognition rate are shown in Table 4. Then, the value of threshold d in the thresholded $L1$ norm in the smooth term was analyzed, as shown in Figure 11. To save time, the EERs in Figure 11 were calculated by utilizing full matching for inter-class and intra-class matching of the first 100 fingers in the PolyU database. Consequently, there are 1500 ($100 \times C_6^2$) intra-class matching and 356400 ($100 \times 6 \times 99 \times 6$) inter-class matching images, respectively.

The results show that the smooth term is essential as suggested in Table 4. The ERR and rank-one recognition of the proposed method are 0.0053 and 0.9940, respectively, which are much more accurate than without the smooth term, without which these values are 0.0145 and 0.9810, respectively. The results demonstrate the importance of the smooth term, which is consistent with the analysis in Section 3. As the value of d varies, different EER values are obtained, thereby indicating that $d = 2$ is the most appropriate choice. This is also consistent with the analysis in Section 3, which determined that $d/\alpha = 4$ is the best neighborhood number frequently employed in a finger vein recognition system.

4.5 Comparison with state-of-the-art methods

In this experiment, we compared the performance of the proposed method with that of various state-of-the-art methods. The compared methods are as follows:

(1) Vessel network-based techniques, which include methods based on mean curvature (MeanC) [11], repeated line tracking (RLT) [12], maximum curvature (MaxC) [28], and even Gabor with morphological (EGM) [13];
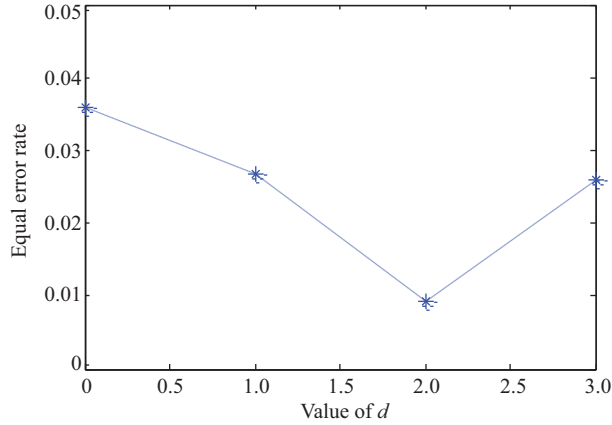
Figure 11 (Color online) Performance when parameter d varies.

Table 5 Performance of different methods on the PolyU database

Method	EER	T-test	
		H	P
LBP [29]	0.0690 ($\pm$ 0.0277)	1	2.90E−05
LLBP [31]	0.0427 ($\pm$ 0.0286)	1	3.65E−04
LDP [32]	0.2241 ($\pm$ 0.0327)	1	1.76E−07
LDC [10]	0.0359 ($\pm$ 0.0331)	1	0.0018
MeanC [11]	0.1064 ($\pm$ 0.0615)	1	2.05E−04
MaxC [28]	0.0265 (−)	−	−
RLT [12]	0.0825 (−)	−	−
EGM [13]	0.0065 (−)	−	−
SIFT [30]	0.0472 ($\pm$ 0.0256)	1	1.18E−04
SPM [33]	0.0357 ($\pm$ 0.0275)	1	6.77E−04
SVDMM [15]	0.0245 ($\pm$ 0.0147)	1	5.06E−04
Proposed method	0.0010 ($\pm$ 0.0035)	−	−

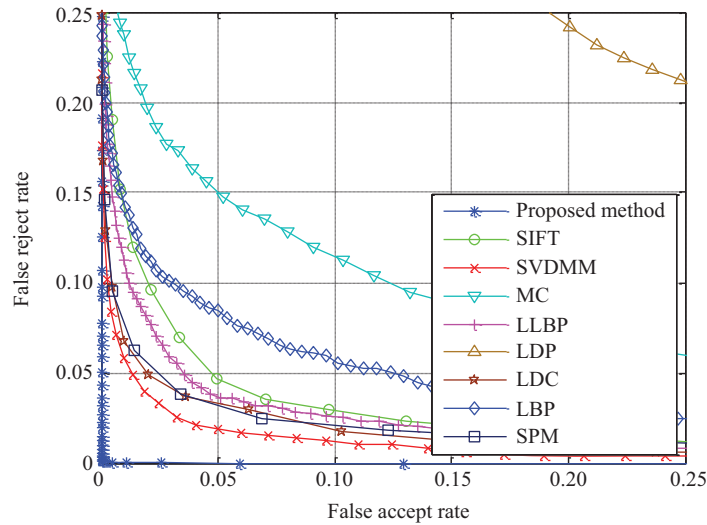− means the value is not provided in the reference paper.

Figure 12 (Color online) ROC curves for different methods.

(2) Local pattern-based techniques, which include methods based on local binary pattern (LBP) [29], local linear binary pattern (LLBP) [31], local derivative pattern (LDP) [32], and local directional code (LDC) [10];

(3) Minutiae-based techniques, which include scale-invariant feature transform (SIFT) [30] and SVDMM [15];

(4) Method based on spatial pyramid matching (SPM) [33], which fused three kinds of features.

To allow for fair comparisons with the baseline algorithm of RLT, MaxC and EGM [13], the PolyU database was utilized in this experiment. Accordingly, the performance was evaluated using a six-fold cross validation and the average fusion was used to calculate the final score for each test image. Because the performance of machine-learning-based methods is not acceptable, it is not listed in this experiment. The average results of EER and statistical t-test are reported in Table 5, with the ROC curves shown in Figure 12.

In the t-test, H indicates the significance of a method. $H=1$ (or -1) means the proposed method is significantly more accurate (or less accurate) than the comparative methods, and $H=0$ represents that the two methods have no significant differences. P is the possibility of rejecting the proposed method as a superior method. The results in Table 5 indicate that the performance of our method is significantly more accurate than all the compared methods at high probability. The average value of EERs of the proposed method is 0.0010, which is the lowest compared with the existing methods, and varies in a small interval. These results demonstrate that the proposed method is superior to state-of-the-art methods.

We also conducted six-fold cross validation on the SDU-MLA database. The EER of the proposed method was 0.0049 with the variance of ± 0.0098. Although the SDU-MLA database is much more difficult for processing purposes, the proposed method achieved a more accurate result than the best existing method [13] listed in Table 5, with an EER of 0.0065 on the PolyU database. This further proves the superiority of the discriminability of the deformation-based method.

5 Conclusion and discussion

Finger vein recognition continues to remain a challenging task because finger vein images are always affected by various deformations. Most of the existing methods focus on the design of deformation invariant features to overcome the problem. Conversely, in our opinion, the deformations can act as useful information and contribute to finger vein recognition. In our paper, we paid attention to the matching operation, and extracted pixel-based displacements to represent various deformations, after which the uniformity of the displacement fields was used to discriminate between genuine and imposter matching. The proposed method was tested on the PolyU and SDU-MLA databases and extensive experiments showed that the deformation information is discriminative.

Actually, the deformation problem not only exists in finger vein recognition. For other biometrics, such as fingerprints [38] and face recognition [39], this problem is also complex and not easy to solve. We plan to explore the possibility of applying this idea to identity authentication based on other biometric patterns in the future.

Conflict of interest   The authors declare that they have no conflict of interest.

References

1   Jain A K, Ross A, Prabhakar S. An introduction to biometric recognition. IEEE Trans Circ Syst Vid, 2004, 14: 4–20

2   Ross A A, Nandakumar K, Jain A K. Handbook of Multibiometrics. Berlin: Springer Science & Business Media, 2006. 6

3   Yanagawa T, Aoki S, Ohyama T. Human finger vein images are diverse and its patterns are useful for personal identification. MHF Prepr Ser, 2007, 12: 1–7

4 Hashimoto J. Finger vein authentication technology and its future. In: Proceedings of 2006 Symposium on VLSI Circuits, Digest of Technical Papers, Honolulu, 2006. 5–8

5 Liu Z, Yin Y, Wang H, et al. Finger vein recognition with manifold learning. J Netw Comput Appl, 2010, 33: 275–282

6 Wu J D, Ye S H. Driver identification using finger-vein patterns with radon transform and neural network. Expert Syst Appl, 2009, 36: 5793–5799

7 Kiyomizu H, Miura N, Miyatake T, et al. Finger vein authentication device. US Patent 8811689, 2014-08-19

8 Sato H. Finger vein authentication apparatus and finger vein authentication method. US Patent 8229179, 2012-07-24

9 Lee E C, Jung H, Kim D. New finger biometric method using near infrared imaging. Sensors, 2011, 11: 2319–2333

10 Meng X, Yang G, Yin Y, et al. Finger vein recognition based on local directional code. Sensors, 2010, 12: 14937–14952

11 Song W, Kim T, Kim H C, et al. A finger-vein verification system using mean curvature. Pattern Recogn Lett, 2011, 32: 1541–1547

12 Miura N, Nagasaka A, Miyatake T. Feature extraction of finger-vein patterns based on repeated line tracking and its application to personal identification. Mach Vision Appl, 2004, 15: 194–203

13 Kumar A, Zhou Y. Human identification using finger images. IEEE Trans Biomed Eng, 2012, 21: 2228–2244

14 Yu C B, Qin H F, Cui Y Z, et al. Finger-vein image recognition combining modified Hausdorff distance with minutiae feature matching. Interdiscip Sci Comput Life Sci, 2009, 1: 280–289

15 Liu F, Yang G, Yin Y, et al. Singular value decomposition based minutiae matching method for finger vein recognition. Neurocomputing, 2014, 145: 75–89

16 Wu J D, Liu C T. Finger-vein pattern identification using principal component analysis and the neural network technique. Expert Syst Appl, 2011, 38: 5423–5427

17 Yang G, Xi X, Yin Y. Finger vein recognition based on $(2d)^2$pca and metric learning. J Biomed Biotech, 2012, 2012: 324249

18 Guan F, Wang K, Liu J, et al. Bi-direction weighted $(2d)^2$pca with eigenvalue normalization one forefinger vein recognition. Pattern Recogn Art Intell, 2011, 24: 417–424

19 Wu J D, Liu C T. Finger-vein pattern identification using svm and neural network technique. Expert Syst Appl, 2011, 38: 14284–14289

20 Yang L, Yang G, Yin Y, et al. A survey of finger vein recognition. In: Proceedings of Chinese Conference on Biometric Recognition. Berlin: Springer, 2014. 234–243

21 Lee E C, Lee H C, Park K R. Finger vein recognition using minutia-based alignment and local binary pattern-based feature extraction. Int J Imag Syst Tech, 2009, 19: 179–186

22 Lee E C, Park K R. Image restoration of skin scattering and optical blurring for finger vein recognition. Opt Laser Eng, 2011, 49: 816–828

23 Mulyono D, Jinn H S. A study of finger vein biometric for personal identification. In: Proceedings of International Symposium on Biometrics and Security Technologies, Islamabad, 2008. 1–8

24 Qin H, Qin L, Xue L, et al. Finger-vein verification based on multi-features fusion. Sensors, 2013, 13: 15048–15067

25 Yang J, Shi Y. Finger–vein roi localization and vein ridge enhancement. Pattern Recogn Lett, 2012, 33: 1569–1579

26 Lu Y, Xie S J, Yoon S, et al. Robust finger vein roi localization based on flexible segmentation. Sensors, 2013, 13: 14339–14366

27 Yang L, Yang G, Yin Y, et al. Sliding window-based region of interest extraction for finger vein images. Sensors, 2013, 13: 3799–3815

28 Miura N, Nagasaka A, Miyatake T. Extraction of finger-vein patterns using maximum curvature points in image profiles. IEICE Trans Inf Syst, 2007, 90: 1185–1194

29 Ojala T, Pietikäinen M, Mäenpää T. Multiresolution gray-scale and rotation invariant texture classification with local binary patterns. IEEE Trans Pattern Anal Mach Intell, 2002, 24: 971–987

30 Pang S, Yin Y, Yang G, et al. Rotation invariant finger vein recognition. In: Proceedings of Chinese Conference on Biometric Recognition. Berlin: Springer, 2012. 151–156

31 Rosdi B A, Shing C W, Suandi S A. Finger vein recognition using local line binary pattern. Sensors, 2011, 11: 11357–11371

32 Zhang B, Gao Y, Zhao S, et al. Local derivative pattern versus local binary pattern: face recognition with high-order local pattern descriptor. IEEE Trans Image Process, 2010, 19: 533–544

33 Xi X, Yang G, Yin Y, et al. Finger vein recognition with personalized feature selection. Sensors, 2013, 13: 11243–11259

34 Liu C, Yuen J, Torralba A, et al. Sift flow: dense correspondence across different scenes. In: Proceedings of European Conference on Computer Vision. Berlin: Springer, 2008. 28–42

35 Lowe D G. Distinctive image features from scale-invariant keypoints. Int J Comput Vision, 2004, 60: 91–110

36 Gonzalez R C, Woods R E, Eddins E L. Digital Image Processing Using MATLAB. Princeton: Pearson Education Inc., 2004

37 Yin Y, Liu L, Sun X. Sdumla-hmt: a multimodal biometric database. In: Proceedings of Chinese Conference on Biometric Recognition. Berlin: Springer, 2011. 260–268

38 Si X, Feng J, Zhou J, et al. Detection and rectification of distorted fingerprints. IEEE Trans Pattern Anal Mach Intell, 2015, 37: 555–568

39 Kim J, Choi J, Yi J, et al. Effective representation using ica for face recognition robust to local distortion and partial occlusion. IEEE Trans Pattern Anal Mach Intell, 2005, 27: 1977–1981